



Probabilistic hazard assessment of the gas emission of Mefite d'Ansanto, Southern Italy

Fabio Dioguardi^{1,2}, Giovanni Chiodini³, Antonio Costa³

¹Dipartimento di Scienze della Terra e Geoambientali, University of Bari "Aldo Moro", Bari, Italy

5 ²The Lyell Centre, British Geological Survey, Edinburgh, United Kingdom

³Sezione di Bologna, Istituto Nazionale di Geofisica e Vulcanologia, Bologna, Italy

Correspondence to: Fabio Dioguardi (fabio.dioguardi@uniba.it)

Abstract. The emission of gas species dangerous for human health and life is a widespread source of hazard in various natural contexts. These mainly include volcanic areas but also non-volcanic geological contexts. A notable example of the latter occurrence is the Mefite d'Ansanto area in the Southern Apennines in Italy. Here, large emissions of carbon dioxide (CO₂) occur at rates that make this the largest non-volcanic CO₂ gas emission in Italy and probably of the Earth. Given the topography of the area, in certain meteorological conditions a cold gas stream forms in the valleys surrounding the emission zone, which proved to be potentially lethal for humans and animals in the past. In this study we present a gas hazard quantification study that considers the main specie, that is CO₂, and the potential effect of the most dangerous, which is hydrogen sulphide (H₂S). For these purposes we used VIGIL, a tool that manages the workflow of gas dispersion simulations specifically optimised for probabilistic hazard applications. Results are discussed and presented in form of maps of CO₂ and H₂S concentration and persistence at various exceedance probabilities considering the gas emission rates and their possible range of variation defined in previous studies.

1 Introduction

20 Carbon dioxide (CO₂), naturally released into the atmosphere, is a gas that can cause harm to humans and animals above certain concentration thresholds and exposure times (e.g., Folch et al., 2017; Settimo et al., 2022; Granieri et al., 2013). In nature, CO₂ can be emitted into the atmosphere by various processes, from slow steady emissions diffuse soil degassing or from volcanic fumaroles (e.g., Chiodini et al., 2021) to catastrophic short-lived large-volume emissions caused by limnic eruptions during lake overturns (e.g., Folch et al., 2017). Other scenarios are possible, like the emission from CO₂ reservoirs in certain geological contexts. This is the case of Mefite d'Ansanto, which represents the largest non-volcanic CO₂ gas emission of Italy and probably of the Earth (Chiodini et al., 2010). In this area in the Southern Apennines (Italy), during periods with stable atmosphere and low winds, the gas, denser than the surrounding air, is channelized at the bottom of a W-E-trending valley, forming a lethal and invisible gas river. The frequent occurrence of the gas river is revealed by the lack of vegetation at the bottom of the valley (Figure 1). Here, dead wild and domestic animals (dogs, cats, foxes, etc.) killed by the high concentration of CO₂ are often found. Furthermore, in the past several lethal accidents involved humans too. Specifically, historical



chronicles of XVII–XVIII century describe the death of nine people (Gambino, 1991). More recently, three persons died in the 1990's (Chiodini et al., 2010).

In this work we use VIGIL (Volcanic Gas dIspersion modeLling, v1.3.7, <https://github.com/BritishGeologicalSurvey/VIGIL/releases/tag/v1.3.7>) (Dioguardi et al., 2022) to carry out a probabilistic hazard assessment of cold CO₂ emissions and streams at Mefite d'Ansanto. VIGIL is a Python tool that manages the gas dispersion simulation workflow for a wide range of applications (single forecast or reanalysis simulation, multiple reanalysis simulations, probabilistic hazard assessment applications). It allows simulating both passive dispersion of a gas specie in the atmosphere by interfacing with DISGAS v2.5.3 (Costa et al., 2009; Costa and Macedonio, 2016) (<http://datasim.ov.ingv.it/models/disgas.html>, hereafter referred to as DISGAS), and dense gas flows on real topography by means of TWODEE-2 v2.6 (Hankin and Britter, 1999; Folch et al., 2009, 2017) (<http://datasim.ov.ingv.it/models/twodee.html>, hereafter referred to as TWODEE-2). In both cases, VIGIL employs DIAGNO v1.5.6 which is a mass consistent wind model modified after DWM (Douglas et al., 1990) (<http://datasim.ov.ingv.it/models/diagno.html>, hereafter referred to as DIAGNO) to simulate the meteorological conditions (wind, temperature gradients) at high resolution in the computational domain starting from observed or modelled meteorological conditions in single locations of the domain. The need to automatically managing the simulation workflow of an atmospheric dispersion application, which is a procedure that involves different and often time-consuming steps (meteorological data retrieval and processing, high-resolution meteorological conditions simulation, gas dispersion simulation, post processing), is particularly evident for Probabilistic Hazard Assessment (PHA) applications, in which a usually large number of simulations are carried out as to explore the uncertainty of selected input parameters (e.g., the wind field, the gas emission rate) (Magill and Blong, 2005; Martí et al., 2008; Neri et al., 2008; Marzocchi et al., 2010; Selva et al., 2010; Sandri et al., 2014; Mead et al., 2022). PHA carried out using gas dispersion models like TWODEE-2 and DISGAS (Costa et al., 2009; Folch et al., 2009; Costa and Macedonio, 2016) is based on multiple deterministic simulations of gas concentration in the area of interest aimed to explore not only the natural variability in input and boundary conditions (seasonal and daily wind variability, source position and gas flux at the emission sources), but also the impact of the uncertainty on other controlling factors such as, for example, the resolution of topographic or meteorological data (Tierz et al., 2016; Selva et al., 2018; Massaro et al., 2021).

For the Mefite d'Ansanto application, Chiodini et al. (2010) performed TWODEE-2 simulations of the CO₂ stream only in very low wind conditions as for the period when they carried out the measurements campaign, which is when the gas river forms. In this work, thanks to the features introduced in VIGIL in v1.3.7, we could explore the uncertainty related to the wide range of meteorological conditions while fixing the CO₂ emission rates to the values reported in Chiodini et al. (2010). In this way we could quantify the probabilistic hazard of the CO₂ concentration in the Mefite d'Ansanto area, without a-priori focusing on the gas river scenario. Furthermore knowing the chemical composition data for the Mefite gas emissions, we could also obtain a first insight on the hazard of hydrogen sulfide (H₂S).



In the following we summarize the geological origin of these steady intense CO₂ emissions in the Mefite d'Ansanto area; then we briefly recall the VIGIL and its capabilities, we present the modelling strategies, the PHA outputs and their implications for the safety of livestock and people in the area.

2 Geological origins of the Mefite d'Ansanto gas emissions

Carbon dioxide dominated gas emissions and groundwaters rich in deeply derived CO₂ affect a large portion of the western side of the Apennine chain at the root of which the gas is thought to be generated by the melting of the carbonates of the subducting Adria plate (Chiodini et al., 2004; Frezzotti et al., 2009; Di Luccio et al., 2022). The Mefite d'Ansanto is the biggest of the numerous gas emissions (>150) located in this sector of the Italian peninsula (www.magadb.net; Chiodini et al., (2010) and references therein). The isotopic signature of He and CO₂ (³He/⁴He ratio expressed as *R/Ra* of 2.58 and $\delta_{13}\text{C}_{\text{CO}_2} = +0.12\text{‰}$ where *Ra* is the helium isotopic ratio in the atmosphere, Table 1) are very similar to those of the fumaroles of the Vesuvio and Campi Flegrei volcanoes ($\delta_{13}\text{C}_{\text{CO}_2}$ from -2‰ to 0.5‰ , *R/Ra* from 2.6 to 3.4; Caliro et al., 2007), a fact that suggested the presence of magmas into the axial part of the sedimentary chain (Italiano et al., 2000; Chiodini et al., 2004). Among the gas species detected in the Mefite gas, it is worth noting the non-negligible presence of hydrogen sulfide (H₂S), which may be harmful or even lethal to humans at relatively low concentrations (<https://www.cdc.gov/niosh/npg/npgd0337.html>; <https://www.cdc.gov/niosh/idlh/default.html>; <https://www.osha.gov/hydrogen-sulfide>) and hence can further increase the gas hazard in the area.

In its ascending towards the surface the gas accumulates in a buried permeable structure made of limestone covered by an impermeable formation. In that zone it forms a gas pocket at a depth of about 1 km (Figure 1). This trap, reached by the Monte Forcuso deep well at 1100-1600 m depth, contains a separated gas phase rich in CO₂ and feeds at the surface the Mefite gas emission (Chiodini et al., 2010 and reference therein).

CO ₂	H ₂ S	N ₂	Ar	He	H ₂	O ₂	CH ₄	$\delta_{13}\text{C}_{\text{CO}_2}$	³ He/ ⁴ He
980000	3580	14300	10.9	16.7	80.7	26	2130	+0.12	2.58

Table 1. Chemical and isotopic composition of Mefite gas (concentrations in $\mu\text{mol/mol}$; Rogie et al., 2000)

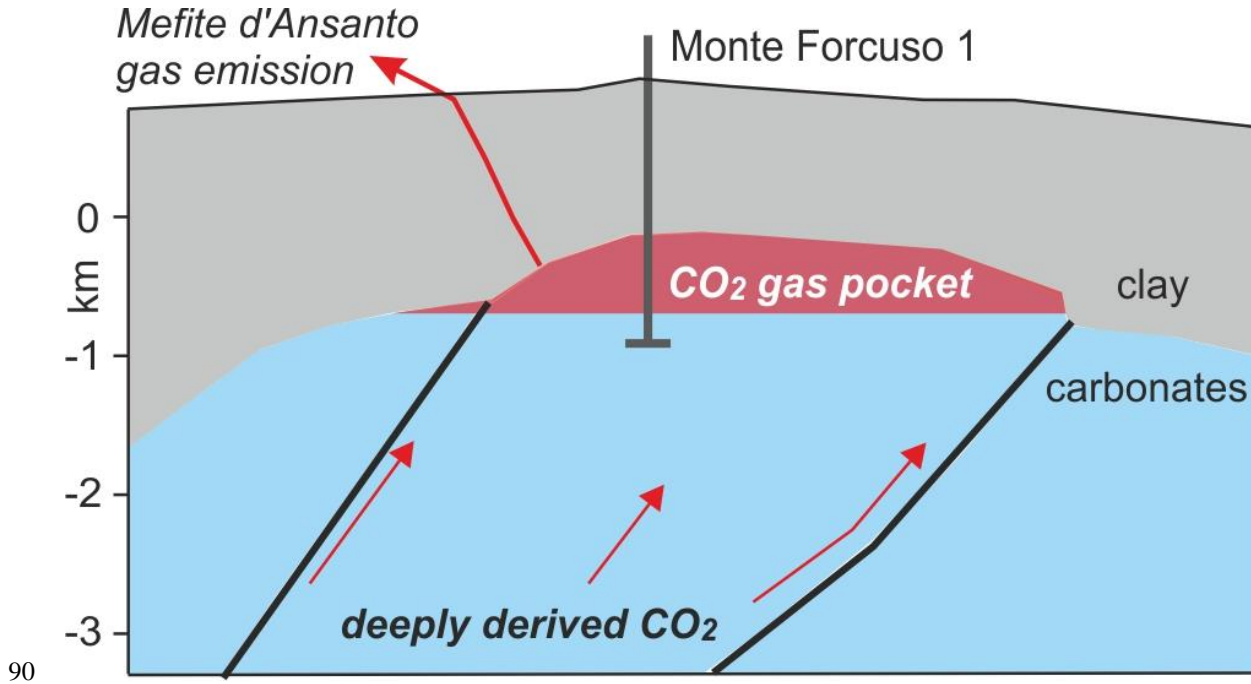


Figure 1. Section of the system feeding Mefite gas emission (redrawn from Chiodini et al. (2010); geological section from Mostardini and Merlini (1986)).

3 Probabilistic hazard assessment at Mefite d'Ansanto using VIGIL

The atmospheric dispersion of a gas emitted by a natural source into the atmosphere is initially controlled by the starting density contrast between the gas and the environment (atmospheric air) and turbulent entrainment of atmospheric air driven by lateral eddies that increase the mixing with air around the edges of the plume, thereby decreasing its bulk density (Costa et al., 2009; Hankin and Britter, 1999; Folch et al., 2009; Costa and Macedonio, 2016). The flow Richardson number at the source Ri is a parameter that takes these factors into account:

$$Ri = \frac{1}{v^2} \left(\frac{g'q}{r} \right)^{\frac{2}{3}} \quad (1)$$

where g' is the reduced gravity:

$$g' = g \frac{\rho_g - \rho_e}{\rho_e} \quad (2)$$

which quantifies the starting buoyancy of the gas phase with starting density ρ_g relative to the environment with density ρ_e . q is the source volumetric flow rate, r is the gas plume radius at the source, which quantifies its extension, and v is the wind speed. Based on the values of Ri , two regimes are possible (Cortis and Oldenburg, 2009; Costa et al., 2013):

- If $Ri < 0.25$, the gas transport is passive and dominated by the wind advection and diffusion (passive dispersion).



- If $Ri > 1$, the gas transport is dominated by the density contrast between the gas and the surrounding environment; in this case the gas flows over the topography until the density contrast persists, being the CO_2 at atmospheric temperature heavier than air.

Although the subsequent atmospheric gas dispersion can be theoretically simulated by solving 3D equations for the conservation of mass, momentum, and energy for each gas species, several scenario-specific simplifications are assumed in practice to reduce the computational time (i.e., single species of gas, incompressible fluid; Costa and Macedonio, 2016), eventually approaching the two end-member scenarios represented by the DISGAS and TWODEE-2 models. In both cases, the momentum coupling with the atmospheric air is taken into account by considering the wind field in the computation domain (simulated with DIAGNO in VIGIL), which is the main factor controlling the light-gas dispersion and one of the controlling factors (together with density contrast) in the heavy-gas case.

DISGAS is an Eulerian model able to simulate the passive dispersal of gases in the atmosphere over complex topographic domains. It assumes that the process is governed by the wind and atmospheric turbulence and solves for the advection-diffusion equation. It is optionally coupled with the meteorological processor DIAGNO, which provides a mass-consistent gridded wind field from meteorological data (“observations”) in the computational domain. DISGAS supports uniform meteorological conditions too, by extrapolating time series of data from a single location in a domain (e.g., a weather station). More details on DISGAS can be found in Costa and Macedonio (2016).

On the other hand, TWODEE-2 code solves a time-dependent model for the flow of a heavy gas based on the shallow layer approach. It is built on the depth-averaged equations for a gas cloud resulting from mixing a gas of density ρ_g with an environment fluid (air) of density ρ_e ($\rho_g > \rho_e$). TWODEE-2 is derived from the optimization and generalization of a previous Fortran-77 version developed by Hankin and Britter (1999). Under the assumption that $h/L \ll 1$ (h being the gas cloud depth and L a characteristic length), the 2D shallow-layer approach allows a compromise between more realistic but computationally demanding 3D CFD models and simpler 1D integral models. Such an approach is able to describe the cloud in terms of four variables: cloud depth, two depth-averaged horizontal velocities, and depth-averaged cloud density as functions of time and position. A full description of the physical model can be found in Folch et al. (2017, 2009). Like DISGAS, TWODEE-2 supports both the uniform wind and DIAGNO options.

3.1 The gas dispersion simulation workflow with VIGIL

VIGIL (Dioguardi et al., 2022) is a Python code designed to manage the simulation workflow required to carry out numerical simulations of atmospheric gas dispersion, i.e.:

1. Retrieving and processing the meteorological data to produce the high-resolution wind field required to simulate atmospheric gas dispersion in the computational domain taking the topography into account via a Digital Elevation Model (DEM);
2. Run the simulation with the gas dispersion model;



3. Process the results to produce new outputs (e.g. probabilistic outputs) and optional plots of gas concentration.

140 3.2.1 Step 1: meteorology

The meteorological data represent the first and most important source of uncertainty variability that VIGIL explores in its current version when PHA is conducted; this implies that, if N realizations of the meteorological conditions are taken into account, VIGIL will run N dispersion simulations. Other sources of uncertainty (e.g., emission rates and gas emission source locations) can also be taken into account on top of the meteorological data variation, i.e., it is possible to apply different gas emission rates to different dispersion simulations, but these will not increase the number of the simulations N , as they are statistically sampled within the N realizations.

The source of the meteorological data depends on the chosen simulation mode (forecast or reanalysis):

- Forecast mode: NCEP (National Centers for Environmental Prediction) Global Forecast System (GFS) Numerical Weather Prediction (NWP) dataset.
- 150 • Reanalysis mode: Copernicus Climate Change Service (C3S), 2023 ERA5 NWP dataset. The user can also provide data manually, for example data from weather stations installed in the computational domain.

GFS and ERA5 are global models with meteorological data saved on a discrete grid with a typical horizontal spacing of approximately 30 km. The typical domain used in the gas dispersion applications under analysis in this work and managed by VIGIL is few km-sided, which means that the NWP data needs to be interpolated into the computational domain. Furthermore, these simulations are generally carried out at a very high spatial resolution (down to few m) in order to capture the gas clouds emitted from point sources (e.g., fumaroles) and the topographic control on gas clouds and cold gas streams. In order to produce reliable simulations of the gas dispersion in these contexts, the simple interpolation into the domain (with the assumption that the meteorological conditions are uniform and equal to the interpolated values throughout the domain) is not sufficient and a high-resolution weather prediction model is used to obtain a realistic wind field at the required spatial resolution starting from the interpolated data. In this step VIGIL, starting from the NWP interpolated data, prepares the input data to run the mass consistent wind model DIAGNO.

3.1.2 Step 2: run the models

In this step, VIGIL runs DIAGNO to obtain the meteorological conditions in the computational domain required by DISGAS and/or TWODEE-2. Subsequently, it runs DISGAS or TWODEE-2 (based on the user's choice). From v1.3.7, a new option that allows the automatic detection of the scenario (light gas or heavy gas), based on the calculation Ri (eq. 1) for each source in the domain, is available. This is very useful in the following situations:

- PHA applications, for which several simulations with varying meteorological conditions are carried out. In this case it is unpractical to manually a-priori determine the correct choice of the scenario and, hence, of the dispersion model (DISGAS or TWODEE-2) for each simulation.



- 170
- Single simulations or PHA applications in which multiple sources with different flow rates are present in the domain. A typical situation may be a domain containing both a weak source representing diffuse degassing, which becomes wind-dominated at very low winds, and a strong source (e.g., a fumarole), which becomes wind-dominated at higher wind speeds. In some situations, each source may behave differently as far as R_i is concerned. In such a situation VIGIL v1.3.7 allows splitting the simulation in a DISGAS and a TWODEE-2 simulation, each one with their correct

175

gas sources. It then merges the outputs of the two simulations. Furthermore, from v1.3.7 VIGIL allows varying the source emission rate using via an ECDF (whose values are provided by the user in a separate input file), a uniform or a gaussian distribution. The latter feature is used in this work.

This new utility exploits a new feature introduced in DIAGNO v1.5.0 that allows tracking the wind speed at locations specified by the user. VIGIL sets the locations at the center of the gas sources.

- 180
- For simplicity, VIGIL v1.3.7 closes the R_i gap between 0.25 and 1 by activating TWODEE-2 when $R_i > 0.25$.

3.1.3 Step 3: post processing of the results

This step deals with the post processing of the DISGAS and/or TWODEE-2 results. Various functionalities are available:

- Conversion between the tracked gas specie into other gas species provided gas species properties (e.g., molar weights, molar ratios between the converted and the tracked species) are available in a separate file.
- 185
- Production of time series of gas concentration at selected locations (tracking points).
- For PHA applications, generation of Empirical Cumulative Density Function (ECDF) of the gas concentration and extrapolation of the gas concentration at the user's desired exceedance probability. The ECDF is calculated by merging, at each point of the domain and for each time step, the concentrations obtained in all simulations using the Python NumPy quantile function.
- 190
- For PHA applications, if gas concentration thresholds and exposure times are provided in input, persistence probability (i.e., the probability to overcome a certain threshold for its exposure time) is calculated.
- For PHA applications, if the tracking points functionality is activated, hazard curves (i.e., exceedance probability vs. gas concentrations) are calculated.

Plots of all these outputs can be optionally generated.

195 4. Numerical simulations of gas flow at Mefite d'Ansanto and probabilistic outputs

4.1. The PHA workflow

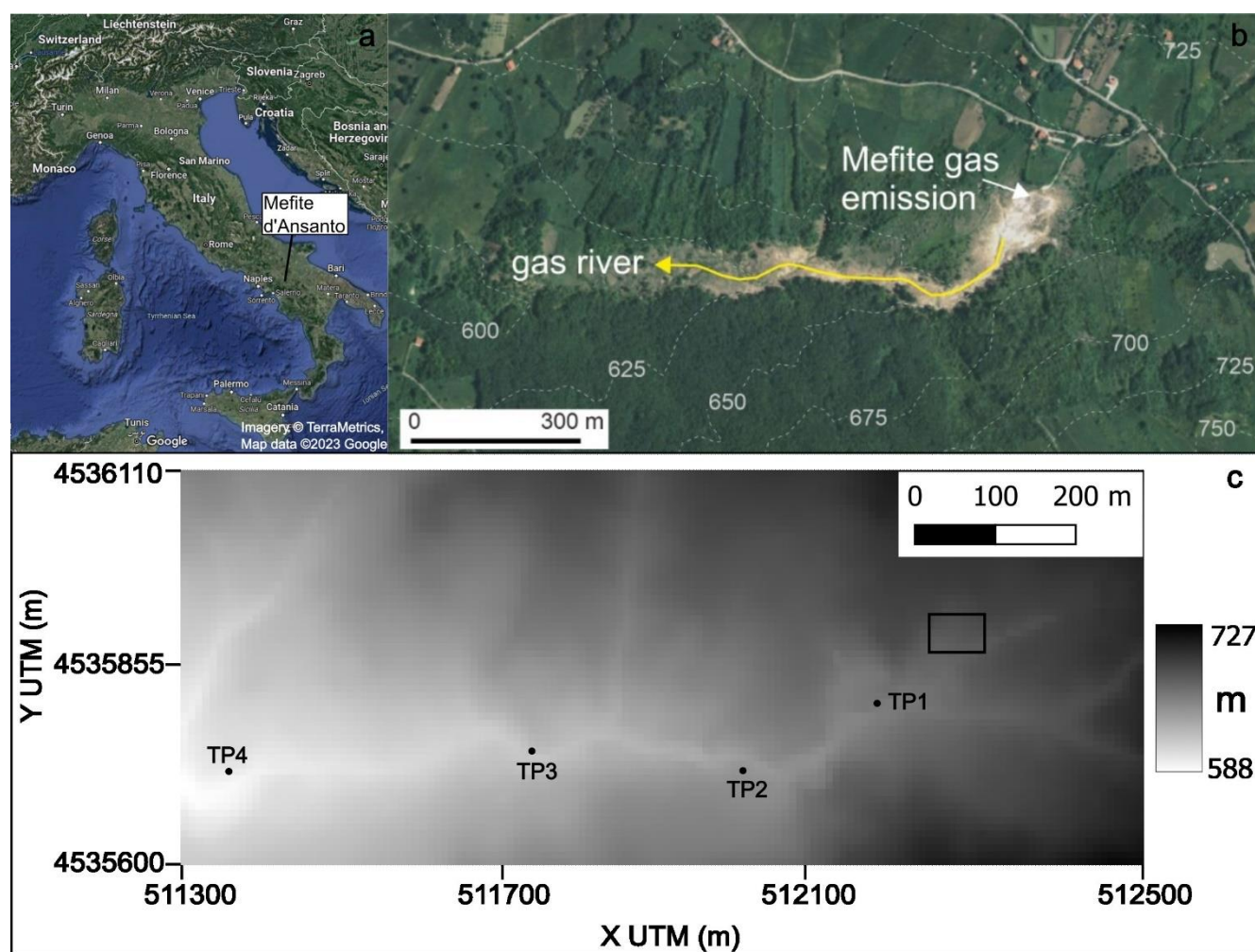
In this section we review the workflow followed to carry out the PHA at Mefite d'Ansanto. All the input files and VIGIL commands required to reproduce the workflow and the outputs are available in the online repository <https://zenodo.org/doi/10.5281/zenodo.10154599>. Details on the input files and commands can be found in the VIGIL User

200

manual and Dioguardi et al. (2022).



We carried out a PHA at Mefite d'Ansanto by exploring the meteorological data variability as the main source of uncertainty and, for each simulation, automatically setting the gas emission rate sampling it from a normal distribution with mean 23.1 kg s^{-1} and standard deviation 5.77 kg s^{-1} according to Chiodini et al. (2010). CO_2 is emitted from an area that can be roughly approximated by a square of 3500 m^2 , which would correspond to a radius r of 33.4 m of the equivalent circle (figure 2).
205 Assuming thermal equilibrium between the emitted gas and the atmosphere, at $15 \text{ }^\circ\text{C}$ the two species (CO_2 and air) have a density ρ of 1.87 and 1.22 kg m^{-3} , respectively. The mean volumetric flow rate q of the gas is therefore $12.35 \text{ m}^3 \text{ s}^{-1}$.



210 **Figure 2:** a) Location of Mefite d'Ansanto in Southern Italy. Imagery © TerraMetrics, Map data ©2023 Google. b) Aerial photo showing the gas emission area and the valley where the gas river forms, which is emphasized by the lack of vegetation (modified after Chiodini et al. (2010)). c) Computational domain with the elevation (m a.s.l.) shown in greyscale. The CO_2 emission area as approximated in the simulations is represented by the black rectangle. Black dots represent the locations of the four tracking points (TP) where the hazard curves are extrapolated from the simulation outputs; the coordinates of the tracking points are listed in Table 2.



215 Meteorological conditions were retrieved from the ERA5 dataset by using the weather.py script of VIGIL. Specifically, since we run one day-long simulations, we sampled 1000 days from the period 01/01/1993 – 01/01/2023 and for each day we downloaded pressure level (Hersbach et al., 2018a) and surface data (Hersbach et al., 2018b) for a location positioned towards the centre of the computational domain. With these data, VIGIL created the input files necessary to run DIAGNO for each day.

220 Subsequently, we executed run_models.py of VIGIL to first obtain the simulated meteorological wind field in the computational domain (figure 1) using DIAGNO. The domain extended from 511300 to 512500 m in the X direction and from 4535600 to 4536110 in the Y direction (UTM coordinates, WGS 84 / UTM zone 33N) and was discretized with 3 m-sized square cells. Then we selected the option to automatically detect which scenario (heavy or light gas) was more appropriate for the simulated day based on the gas emission characteristics and the wind conditions at the source location. In

225 fact, with these gas source emission characteristics described above, the gas source satisfies the conditions of the heavy gas regime in case of very low to no-wind conditions. Specifically, based on eq. 1, the maximum wind v that would satisfy the heavy gas regime ($Ri > 1$) would be 1.25 m s^{-1} . With a wind of 2.49 m s^{-1} the passive wind-dominated conditions ($Ri < 0.25$) would be already satisfied. It resulted that 312 over 1000 runs could be simulated with TWODEE-2 (heavy gas scenario) and the rest (611 simulations) with DISGAS.

230 Finally, we run post_process.py to produce the requested outputs. Specifically, we requested:

- ECDFs' 50%, 16% and 5% exceedance probability of the CO_2 concentration at 2 m above the ground for the time-averaged solution over the whole simulation duration (24 hours). Furthermore, by means of the gas specie conversion capability of VIGIL, we calculated the same outputs for H_2S by using the chemical composition data listed in Table 1, specifically the molar ratio between H_2S and CO_2 (0.0036).

235 It is worth noting that the current version of VIGIL does not allow starting the simulation from a pre-existent solution of the gas concentration field, i.e., each simulation starts with clean air (apart from background concentrations that the user may specify). This may affect the simulations' outputs in the initial time steps in scenarios like those under analysis in this work, i.e., with a steady long-lived gas emission. However, in a small domain like the one under consideration in this research, the CO_2 cloud or stream can be considered fully developed

240 within the first hour, which is the minimum time resolution for outputs currently allowed by VIGIL. Therefore, we can safely assume that the effect of starting from clear air is negligible in this application when we calculate the 24-hour time-average of the outputs.

- Persistence outputs, the probability to overcome the concentration thresholds for their respective times as specified in the input file specifying the gas property (gas_properties.csv). The concentration thresholds and exposure times

245 for CO_2 used in this work are listed in Table 1 and are compiled based on Costa et al. (2008), Granieri et al. (2013), Settimo et al. (2022) and references therein. For 1000 and 3500 ppm there are no time exposure indicated, therefore we calculate the persistence for 24 hours. For 5000 ppm, TWA (Time Weighted Average) values for CO_2 are commonly used in occupational health and safety to establish permissible exposure limits or recommended



250 exposure limits. These limits define the maximum allowable concentration of CO₂ that a worker or individual can
 be exposed to over a specific time period, usually 8 hours or 24 hours. In this work we take 8 hours as exposure
 time. For the highest concentrations taken into account (15000, 30000 and 100000), the exposure times that cause
 harm are always in the range of 10-15 minutes, with the effects on humans listed in the table. In this study, for
 computational limitations, as reported in Table 2, the minimum exposure time we considered is 1 hour. For H₂S we
 used the thresholds and exposure times defined by the United States Occupational Safety and Health Administration
 255 (OSHA) (<https://www.osha.gov/hydrogen-sulfide/>), based on the recommendations of The National Institute for
 Occupational Safety and Health (NIOSH) (<https://www.cdc.gov/niosh/idlh/default.html>;
<https://www.cdc.gov/niosh/npg/npgd0337.html>) and the base threshold defined in Olafsdottir and Gardarsson,
 (2013). OSHA defines three limits: Recommended Exposure Limit (REL), Permissible Exposure Limit (PEL) and
 Immediately Dangerous to Life and Health (IDLH) exposure limit.

260

CO ₂ concentration threshold (ppm)	Exposure time in the literature and effects	Exposure time in this work (hours)
1000	no time indicated: no effects under this threshold (Settimo et al., 2022)	24
3500	no time indicated: no effects if ventilated ambient (Granieri et al., 2013)	24
5000	TWA 8 hours (Costa et al., 2008; Granieri et al., 2013). Above TWA: Slight increase in breathing rate	8
15000	Above 10 minutes: Breathing deeper and more frequent (Costa et al., 2008; Granieri et al., 2013)	1
30000	Above 15 minutes: Breathing increases to twice normal rate, weak narcotic effect, headache for long time exposure (Costa et al., 2008; Granieri et al., 2013)	1
100000	Respiratory distress with loss of consciousness in 10–15 min (Costa et al., 2008; Granieri et al., 2013)	1

Table 2. CO₂ concentration thresholds and exposure times that can cause harm to humans

265



H ₂ S concentration threshold (ppm)	Exposure time in the literature and effects	Exposure time in this work (hours)
0.035	No effects under this threshold [REF]	24
10	Construction 8-hour Limit; Shipyard 8-hour limit: 10 ppm (OSHA PEL)	8
50	General Industry Peak Limit (OSHA PEL), 10 minutes. At 50-100 ppm, possible effects include slight conjunctivitis ("gas eye") and respiratory tract irritation after 1 hour. May cause digestive upset and loss of appetite.	1
100	NIOSH IDLH. Coughing, eye irritation, loss of smell after 2-15 minutes (olfactory fatigue). Altered breathing, drowsiness after 15-30 minutes. Throat irritation after 1 hour. Gradual increase in severity of symptoms over several hours. Death may occur after 48 hours (OSHA).	1
500	Staggering, collapse in 5 minutes. Serious damage to the eyes in 30 minutes. Death after 30-60 minutes. (OSHA)	1

Table 3. H₂S concentration thresholds and exposure times that can cause harm to humans

- Hazard curves, i.e., exceedance probability vs. CO₂ concentration plots, at four selected locations or tracking points (TP, see Figure 2) spread along the valley. Table 4 lists the coordinates of the four tracking points:

270

TP#	X UTM (m)	Y UTM (m)	Z (m above the ground)
1	512181	4535810	2.0
2	512022	4535724	2.0
3	511772	4535749	2.0
4	511413	4535723	2.0

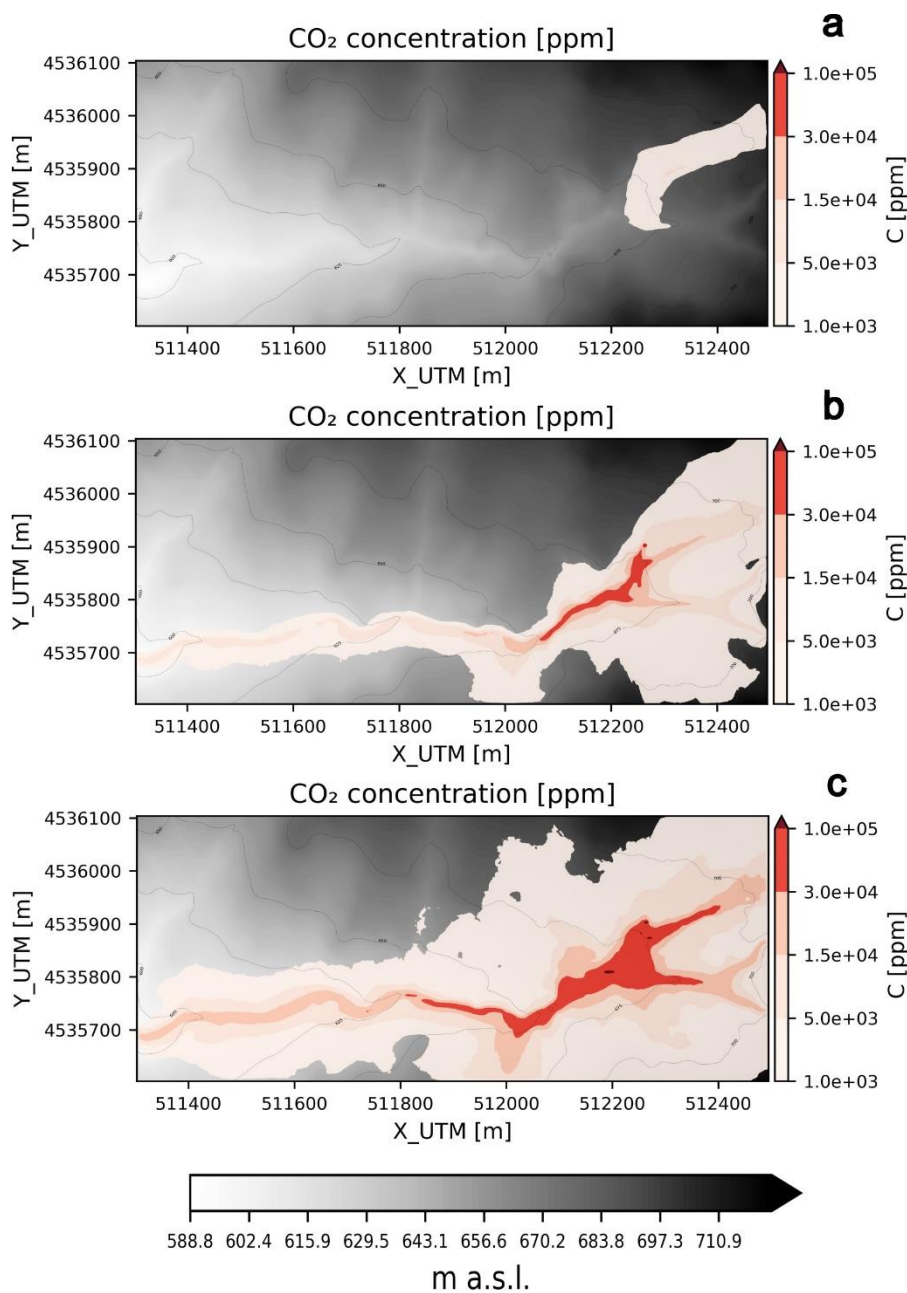
Table 4. Coordinates (UTM) and elevations (m above the ground) of the four tracking points used for the hazard curves



275 We also carried out a seasonal analysis, i.e., we produced the aforementioned outputs for each season (winter, spring, autumn, summer) to check if there is a control of the season on the CO₂ dispersion pattern.

4.2. Results

Figure 3 shows the concentration of CO₂ in the domain at 2 m above the ground at 50%, 16% and 5% exceedance probability. The concentration is obtained by interrogating the ECDF of the 24-hours time-averaged solution in each point of the domain.



280 **Figure 3.** 24 hours time-averaged CO₂ concentration at 2 m above the ground at 50% (a), 16% (b) and 5% (c) exceedance
285 probabilities

At 50% exceedance probability (figure 3a), which corresponds to the median of the ECDF, non-negligible to high (few
thousands of ppm) concentrations of CO₂ are visible in the emission area and towards the eastern part of the domain. These
285 areas are uphill the emission area, which means that on average elevated CO₂ levels caused by the action of finds blowing



from W-SW cannot be ruled out. At 16% exceedance probability (figure 3b), which corresponds to the median + 1 standard deviations of the ECDF, the CO₂ concentration significantly increases up to dangerous levels (> 15,000 ppm) and the streams along the valleys become visible. By further decreasing the exceedance probability to 5%, which corresponds to the median + 2 standard deviations of the ECDF (figures 3c), the extent of the areas affected by CO₂ concentration > 15,000 ppm further
290 increase and eventually the areas become not confined to the valleys. Areas affected by CO₂ concentration > 30,000 ppm extend significantly outside the emission area at 5% exceedance probability.

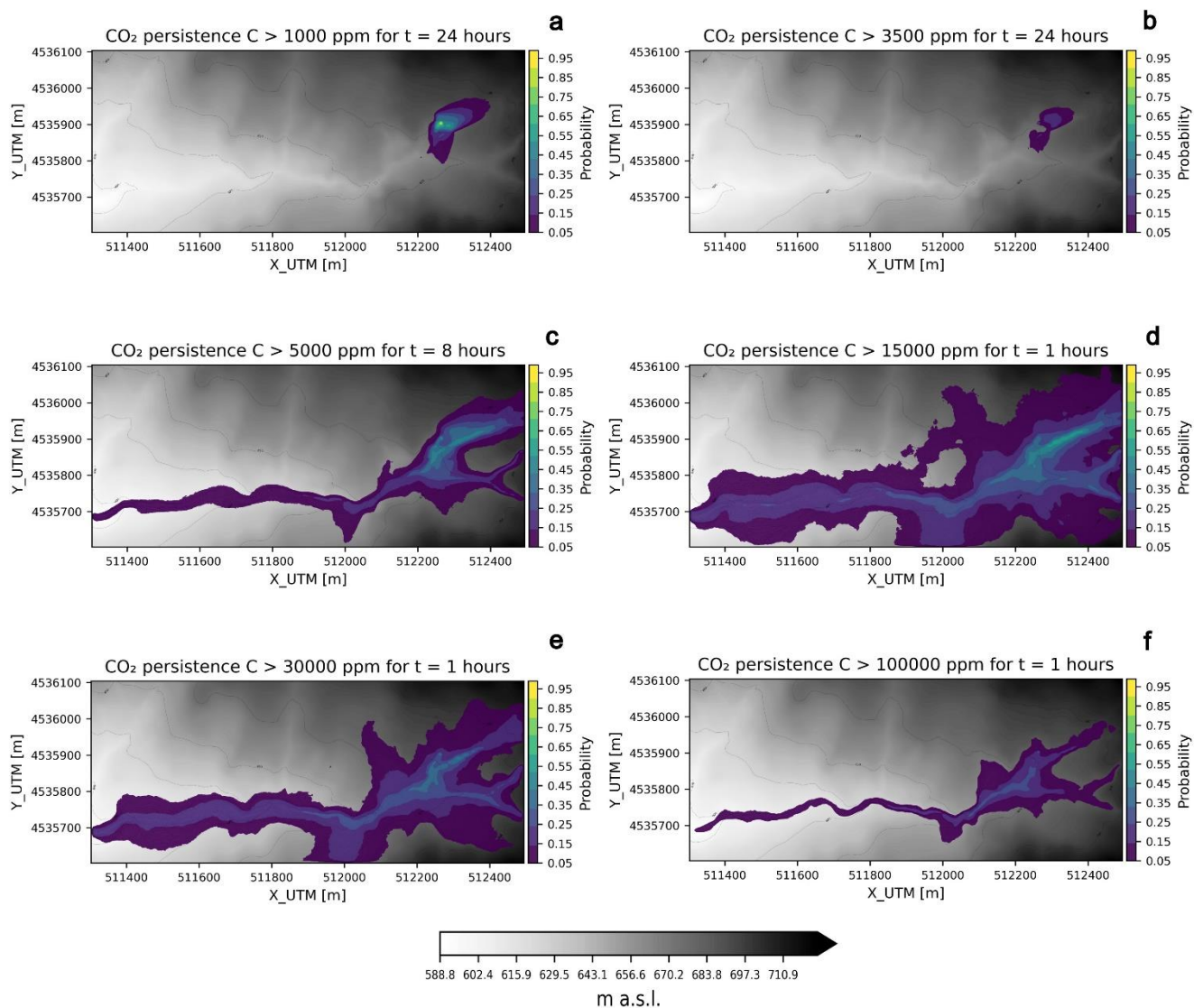
Figure 4 displays the persistence maps for the six concentration thresholds and exposure times listed in Table 2. All probabilities are calculated at 2 m above the ground. Figure 4a shows the probability to overcome a CO₂ concentration of 1,000 ppm for at least 24 hours, which is the duration of the simulation. This probability is high in the emission area but is also not
295 negligible (5 - 10%) along the main E-W valley and some areas towards NE in the domain. This is in line with what is observed in figure 3a, which was interpreted as the formation of CO₂ plumes drifting NE due to the action of winds blowing from W-SW. Figure 4b shows the probability to overcome a CO₂ concentration of 3,500 ppm for at least 24 hours. As expected, the probability is lower than the case shown in figure 3a but still not negligible along the main valley and in the emission area and surroundings. Considering an exposure time of 8 hours, the probability to overcome a CO₂ concentration of 5,000 ppm is high
300 in the emission area and surroundings (up to 50%), lower but still notable towards E-NE (up to 30%) and not negligible along most of the valleys (10 - 20%) (figure 4c). Focusing on high (15,000 – 30,000 ppm) to very high (100,000) concentrations for an exposure time of 1 hour (figure 4d, 4e and 4f, respectively), the extent of the domain affected by significant probabilities is noteworthy for 15,000 ppm and 30,000, with probabilities up to 50% - 60% in the emission area and surroundings (particularly towards NE) and along the valleys (up to 20 – 30%). Even in the most extreme case of CO₂ concentrations > 100,000 ppm
305 there is a 30% probability to overcome this concentration for 1 hour in the emission area and surroundings and a not negligible (up to 10 – 20 %) one along the valleys.

The hazard curves produced at the four locations identified by the four tracking points listed in Table 3 and shown in figure 2 are represented in figure 5. In the location TP1, which is the closest one to the emission area, higher concentrations of CO₂ than the other locations are expected, i.e., for a fixed exceedance probability the concentration is significantly higher. The
310 maximum concentration is close to 140,000 ppm. The curves at the other locations show similar values, though slightly higher for TP2, which is the second closest to the emission area. By looking at figure 2c, TP2, TP3 and TP4 are positioned along the main W-E valley. The fact that the concentrations are almost the same, especially in TP3 and TP4, can be interpreted as the CO₂ stream maintaining its characteristics along the valley, at least in the analysed domain.

We wanted to check if there is a seasonal control on the simulations output, i.e., the predicted concentrations differ significantly
315 among the four seasons. We first split the dataset of simulations in four categories based on the month of each simulated day: winter (December, January and February), spring (March, April, May), summer (June, July, August) and autumn (September, October, November). For each season, we computed the same outputs (ECDFs and persistence) as those shown in figures 3 and 4. In particular, figure 6 shows the 24 hours' time-averaged CO₂ concentration at an exceedance probability of 16% for the four seasons. The concentrations are significantly higher in the summer season, followed by autumn. Winter and spring



320 are characterized by similarly lower concentrations, although the concentrations are slightly lower in winter than in spring. A
closer look at the plots also shows how the summer is characterized by significantly higher values of CO₂ concentration in the
main W-E valley (figure 6c), followed by autumn (figure 6d). In order to better understand this seasonal control, which in our
hypothesis depends on the wind speeds, we calculated the 24 hours' time-averaged average wind speed in the domain at 10 m
above the ground for each day and then, by collecting these data for each season, we calculated the ECDF of this averaged
325 wind speed. Figure 7 shows the 24 hours' time-averaged average wind speed vs. the exceedance probability. Upon a first look
at the four curves, it is evident how the wind speed is significantly lower in the summer (grey solid line), followed by the
autumn (yellow solid line). The other two seasons display similar trends, although spring (orange solid line) is characterized
by lower winds, particularly at exceedance probabilities lower than 50%. Summarizing the findings shown in figure 7, it is
more likely to experience higher wind intensities and hence lower concentrations in winter, followed by spring and autumn.
330 Summer shows the lowest winds and the highest concentrations.



335 **Figure 4.** Persistence maps at 2 m above the ground. a) Concentration threshold = 1000 ppm, exposure time = 24 hours. b) Concentration threshold = 3500 ppm, exposure time = 24 hours. c) Concentration threshold = 5000 ppm, exposure time = 8 hours. d) Concentration threshold = 15000 ppm, exposure time = 1 hour. e) Concentration threshold = 30000 ppm, exposure time = 1 hour. f) Concentration threshold = 100000 ppm, exposure time = 1 hour.

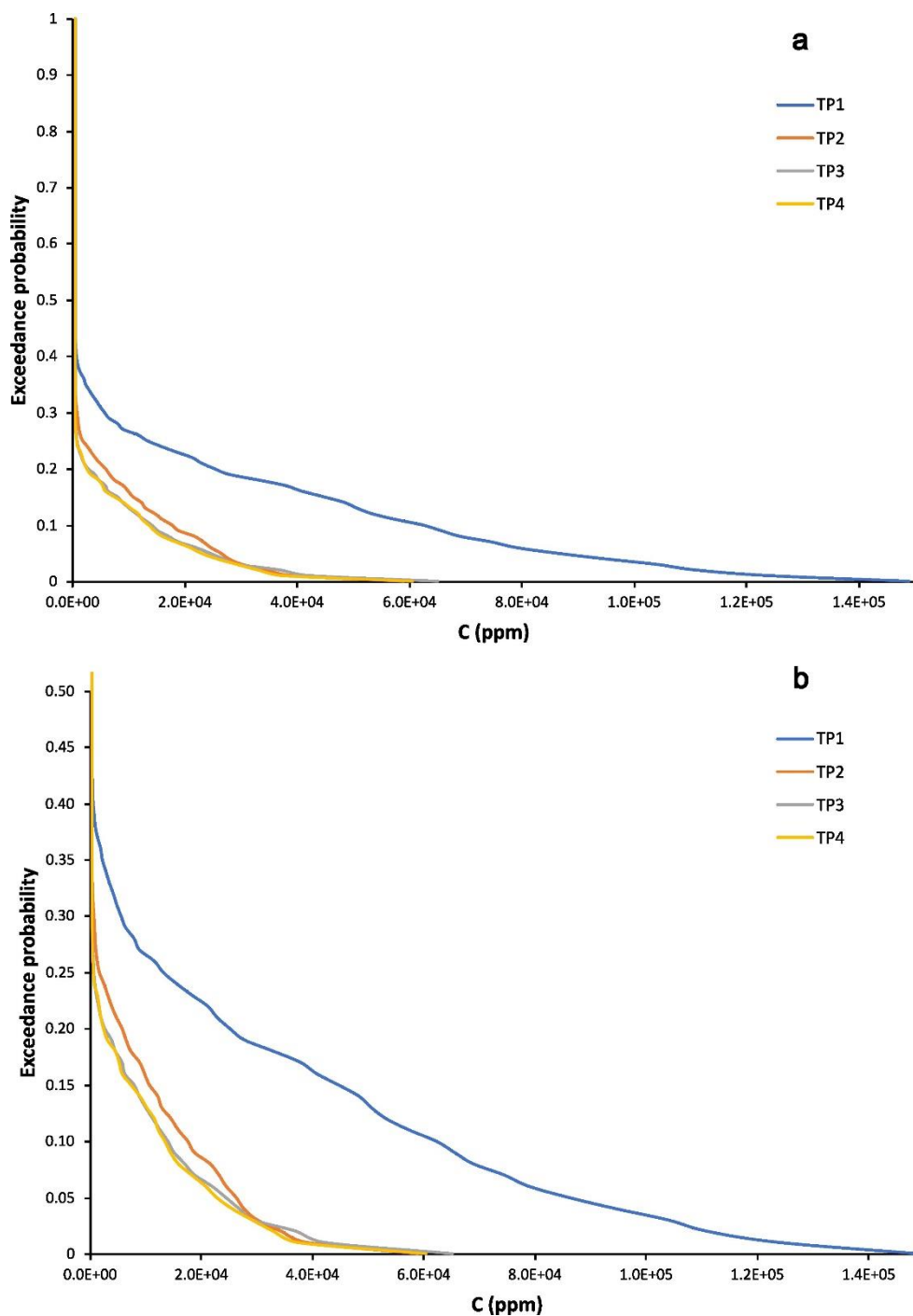
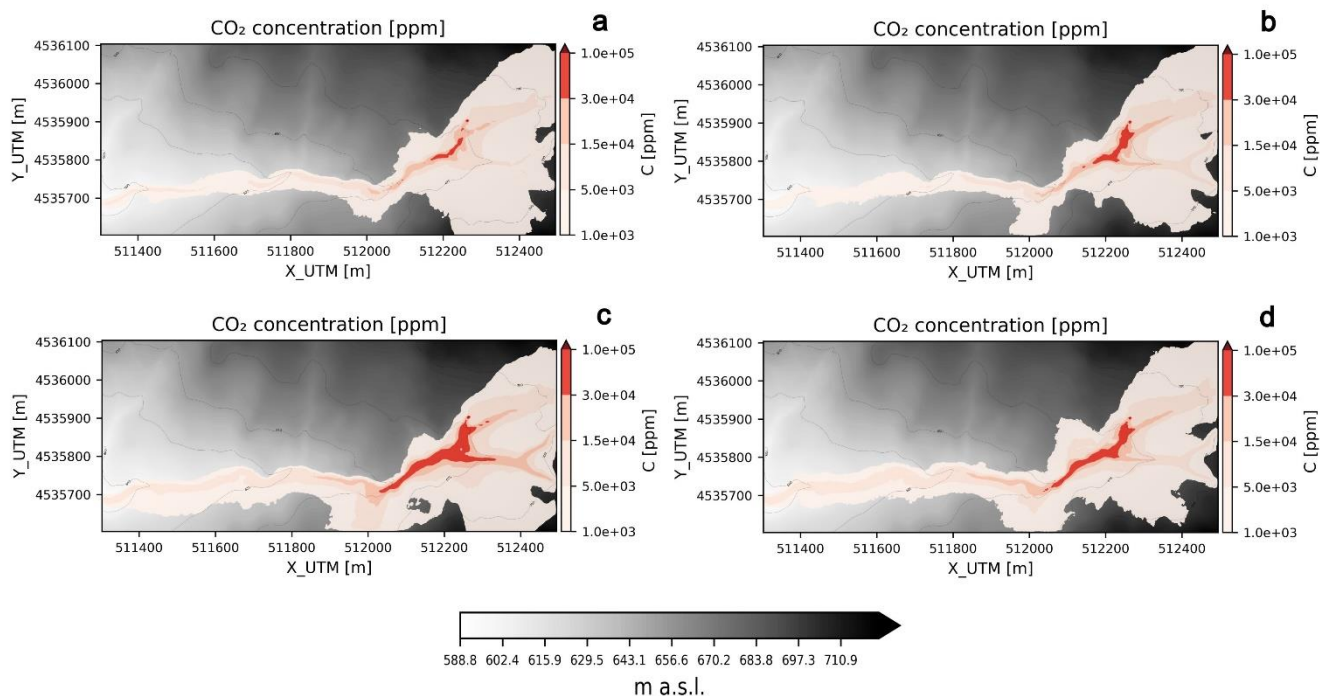
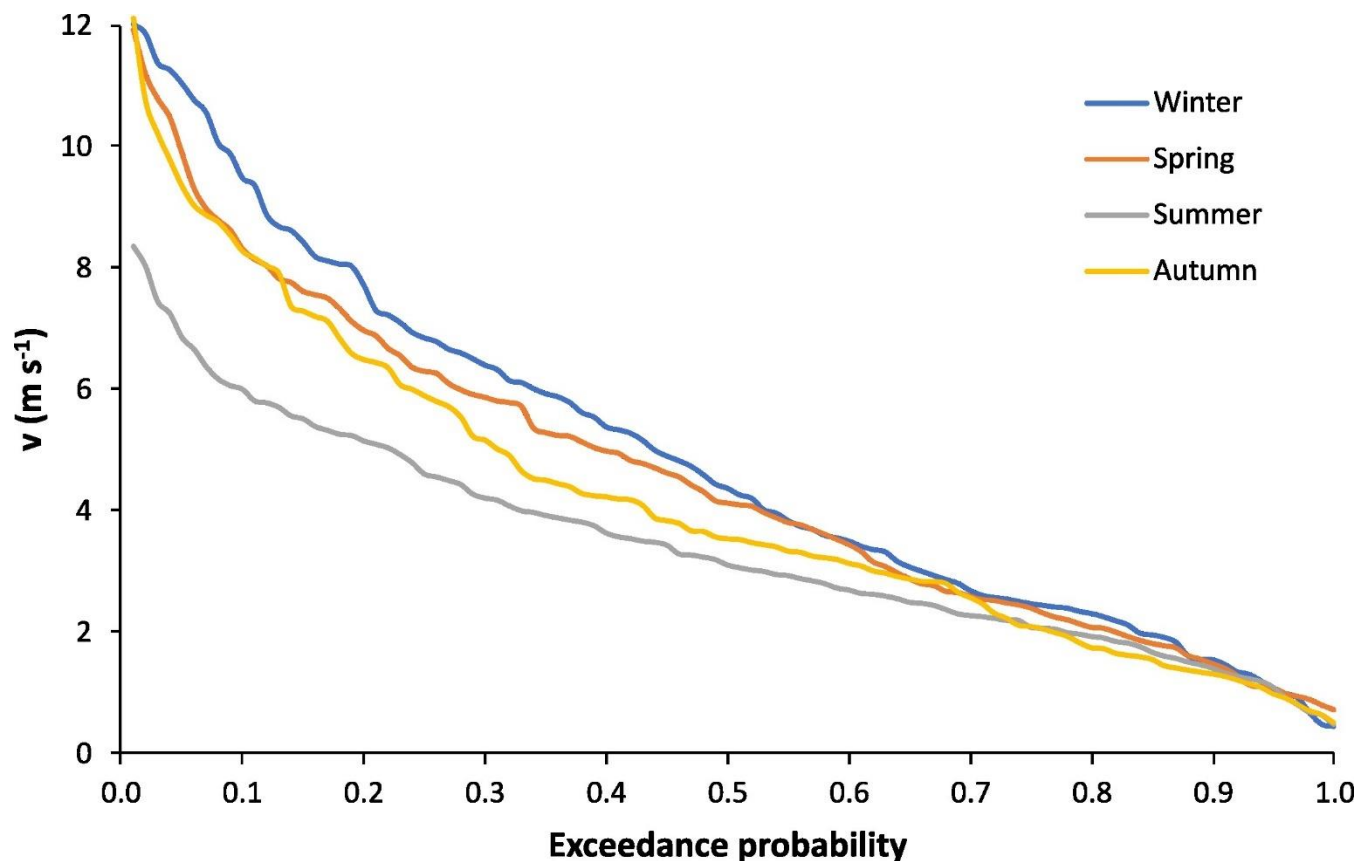


Figure 5. Hazard curves at the four locations identified by the four tracking points. The hazard curves for the tracking points 1, 2, 3 and 4 are represented by the blue, orange, grey and yellow solid line, respectively. a) Plot in the original scale used by VIGIL. b) Zoomed version.



340

Figure 6. 24 hours' time-averaged CO₂ concentration at 2 m above the ground at 16% exceedance probability for the four seasons: a) winter; b) spring; c) summer; d) autumn.



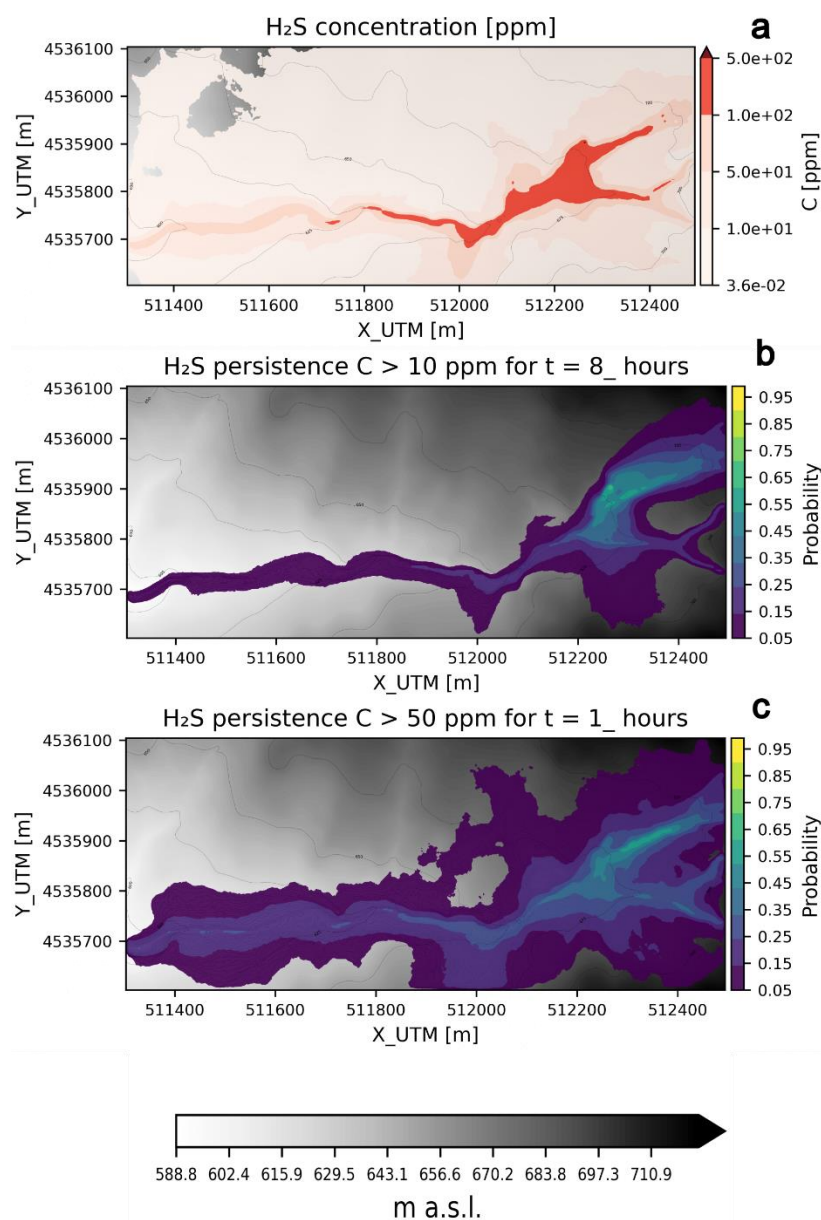
345 **Figure 7.** ECDF of the 24 hours' time-averaged domain-averaged wind speed at 10 m above the ground for winter (solid blue line), spring (solid orange line), summer (solid grey line) and autumn (solid yellow line).

It is also worth noting that the probabilities for winds lower than 3 m s^{-1} are very similar, as for the highest winds (appx. 12 m s^{-1}), although in the latter case the summer never reaches winds higher than 9 m s^{-1} . The results of this analysis of the meteorological conditions explain the seasonal differences shown in Figure 6. In the summer, when high winds are less likely than the other seasons, it is more likely to form a dense gas flow river in the valleys and to have higher concentrations in the areas surrounding the gas source. Autumn shows a similar pattern, although with a slightly lower probability to produce a
350 dense gas flow in the valleys. This likelihood becomes significantly lower in the autumn and spring.

Finally, figure 8 shows some of the probabilistic outputs produced for the H_2S gas specie and the concentration thresholds and exposure times listed in Table 3. The map of H_2S concentration at 2 m above the ground at an exceedance probability of 5% shows levels of H_2S above one of the PEL ($>50 \text{ ppm}$) along all the valleys and the emission area. Dangerous levels (>100
355 ppm) are also significantly widespread in the emission area and the adjacent sectors of the valleys. Figure 8b and c displays the persistence maps for two PELs (10 ppm for 8 hours and 50 ppm for 1 hour, see Table 4). The probability to overcome these levels for the defined time intervals are significant in the same areas, reaching up to 50-60% in the vicinity of the emission zone for both PELs. The probability to overcome 50 ppm for 1 hour is up to 30% even 800-1000 m away from the gas source



360 in the main W-E valley. Therefore, whilst further H₂S-specific measurement campaigns are required in order to draw conclusions on the H₂S hazard, these results show that the H₂S hazard should also be taken into account on top of the CO₂ one.



365 **Figure 8.** H₂S probabilistic hazard maps at 2 m above the ground. a) 24 hours' time-averaged concentration at 5% exceedance probability. b) Persistence maps for PEL 10 ppm, exposure time = 8 hours. c) Persistence maps for PEL 50 ppm, exposure time = 1 hour.



5. Discussion

The analysis carried out with VIGIL confirmed that the computational domain under analysis is prone to non-negligible likelihoods to be exposed to high concentrations of CO₂. This is particularly evident in the areas surrounding the gas source and the valleys, especially the main W-E valley where the generation of a CO₂ gas river is a well-known occurrence and marked by the absence of vegetation at the lowermost levels.

By looking at the 50th percentile of the solutions (50% exceedance probability of the ECDF generated by VIGIL, Figure 3), one can observe that on average the source area and the area towards NE from the emission zone is the most affected one, with 24 hours' time-averaged CO₂ concentrations up to few thousand ppm. The generation of the cold gas river in the valleys of the domain is observed at lower exceedance probabilities, which implies that this occurrence is less likely. However, the gas river is already well visible at 16% exceedance probability with very high CO₂ concentrations (>15,000 ppm) in many areas of the valleys and source area and surroundings. This means that there is the 16% probability to have even worse scenarios, which is not a low likelihood. In fact, at lower exceedance probabilities (5%) the scenarios look significantly worse. The persistence maps (Figure 4), created by VIGIL based on the concentration thresholds and related exposure times of Table 2, corroborates these findings. Likelihoods to overcome dangerous CO₂ concentrations levels for specified times are non-negligible to significant. For example, for concentrations of 30,000 and 100,000 ppm, which are dangerous to very dangerous for the humans' health even for exposure times of few minutes, the probability to overcome these thresholds for 1 hour are significant (up to 40-50 %) especially in the emission area and the valleys' segment close to the gas source. It is worth noting that the exposure times for these two concentrations thresholds are set to 10-15 minutes (Table 2), but we could calculate the persistence for time intervals of at least 1 hour the current computational limitations, which imposes the minimum time step to 1 hour. This means that the probabilities shown in Figure 4 (d, e, f) would likely be even higher if the proper exposure times (10-15 minutes, Table 2) would have been taken into account. Therefore, our persistence calculations results represent a safe lower estimate than the real one.

Similar considerations can be done for H₂S (Figure 8), whose concentrations in our study were estimated by means of the gas composition data (Table 1) and the specie conversion capability of VIGIL. Results shown in figure 8 (H₂S concentration at an exceedance probability of 5% and persistence maps based on the PEL defined in Table 3) demonstrated that the hazard posed by H₂S cannot be discarded in the area and should be taken into account on top of the CO₂ for assessing the gas hazard in this area.

6. Conclusions

In this work we presented results of the first PHA carried out at Mefite d'Ansanto, the largest non-volcanic CO₂ gas emission of Italy and probably of the Earth. To do so, we used VIGIL v1.3.7, a Python tool designed to manage the workflow of gas dispersion simulations and post-processing, specifically designed to carry out PHA applications. Thanks to VIGIL, we could run 1,000 simulations of CO₂ gas dispersion in the area, with each simulation representing the 24 hours-long dispersion on a



day randomly sampled from the period 01/01/1993 – 01/01/2023. The meteorological data retrieved by VIGIL from the ERA5
400 dataset (Hersbach et al., 2018a, b) were used to compute the wind field at high resolution by means of DIAGNO. Then, for
each simulation day we:

- varied the gas emission rate sampling it from a normal distribution with mean 23.1 kg s^{-1} and standard deviation 5.77 kg s^{-1} according to Chiodini et al. (2010);
- evaluated the daily-averaged Richardson number at the source was evaluated and, based on its value, through VIGIL
405 we carried out the simulation with DISGAS or TWODEE-2. In this way we were not forced to use one of the two
models for all the simulations or to manually select the model to use for each day.
- Finally, the post-processing capabilities of VIGIL allowed us to produce hazard maps, hazard curves and persistence
410 maps, which highlighted the occurrence of potentially dangerous concentrations of CO_2 at low levels in the
atmosphere at non-negligible likelihoods. This is not a surprise, since fatalities occurred in the past and the main W-
E valley in the considered domain is characterized by the lack of vegetation, which indicates the recurrent occurrence
of the cold CO_2 gas stream. We could also obtain preliminary indications on the H_2S hazard in the area, which should
not be discarded and should be further tackled in future studies.

Future developments of VIGIL will allow better treating the uncertainty of the source (both in the location and strength) and
assessing the probability of death depending on exposure duration, following the approach of Folch et al. (2017), who
415 computed the percentage of human fatalities based on a probability density that depends on concentration thresholds and
exposure times of the selected gas specie. Furthermore, we plan to use a more up-to-date wind processor that enables time
steps shorter than one hour, which is the current limit due to the use of DIAGNO. This in turn will allow improving the analysis
of the impact of gas species concentrations on human health, since some of the concentration thresholds are related to exposure
time of few minutes. In this way, we should also be able to produce more sophisticated probabilistic outputs of the impact of
420 human health.

Code availability

VIGIL v1.3.7, with which the PHA was carried out, is available at
<https://github.com/BritishGeologicalSurvey/VIGIL/releases/tag/v1.3.7>.

Data availability

425 All the data and instructions necessary to replicate the presented PHA are available at
<https://zenodo.org/doi/10.5281/zenodo.10154599>. The repository also includes all the probabilistic outputs generated by
VIGIL.



Author contribution

FD contributed to the conceptualization, data curation, formal analysis, simulations, software development, visualization and
430 writing. AC and GC contributed to the conceptualization, formal analysis and writing.

Competing interests

The authors declare that they have no conflict of interest.

Acknowledgements

Hersbach et al., 2018 was downloaded from the Copernicus Climate Change Service (C3S) (2023). The results contain
435 modified Copernicus Climate Change Service information 2020. Neither the European Commission nor ECMWF is
responsible for any use that may be made of the Copernicus information or data it contains. This work is published with
permission of the Executive Director of British Geological Survey (UKRI). This study was carried out within the RETURN
Extended Partnership and received funding from the European Union Next-GenerationEU (National Recovery and Resilience
Plan – NRRP, Mission 4, Component 2, Investment 1.3 – D.D. 1243 2/8/2022, PE0000005). This work was partially supported
440 by the INGV Project FURTHER.

References

- Caliro, S., Chiodini, G., Moretti, R., Avino, R., Granieri, D., Russo, M., and Fiebig, J.: The origin of the fumaroles of La
Solfatara (Campi Flegrei, South Italy), *Geochim Cosmochim Acta*, 71, 3040–3055, <https://doi.org/10.1016/j.gca.2007.04.007>,
2007.
- 445 Chiodini, G., Cardellini, C., Amato, A., Boschi, E., Caliro, S., Frondini, F., and Ventura, G.: Carbon dioxide Earth degassing
and seismogenesis in central and southern Italy, *Geophys Res Lett*, 31, <https://doi.org/10.1029/2004GL019480>, 2004.
- Chiodini, G., Granieri, D., Avino, R., Caliro, S., Costa, A., Minopoli, C., and Vilardo, G.: Non-volcanic CO₂ Earth degassing:
Case of Mefite d' Ansanto (southern Apennines), Italy, *Geophys Res Lett*, 37, L11303, <https://doi.org/10.1029/2010GL042858>,
2010.
- 450 Chiodini, G., Caliro, S., Avino, R., Bini, G., Giudicepietro, F., De Cesare, W., Ricciolino, P., Aiuppa, A., Cardellini, C.,
Petrillo, Z., Selva, J., Siniscalchi, A., and Tripaldi, S.: Hydrothermal pressure-temperature control on CO₂ emissions and
seismicity at Campi Flegrei (Italy), *Journal of Volcanology and Geothermal Research*, 414, 107245,
<https://doi.org/10.1016/j.jvolgeores.2021.107245>, 2021.
- Copernicus Climate Change Service (C3S): ERA5 hourly data on single levels from 1940 to present. Copernicus Climate
455 Change Service (C3S) Climate Data Store (CDS). (Accessed on 28-JUL-2023), 2023.



- Cortis, A. and Oldenburg, C. M.: Short-Range Atmospheric Dispersion of Carbon Dioxide, *Boundary Layer Meteorol*, 133, 17–34, <https://doi.org/10.1007/s10546-009-9418-y>, 2009.
- Costa, A. and Macedonio, G.: DISGAS: a model for passive DISpersion of GAS, 332 pp., 2016.
- Costa, A., Chiodini, G., Granieri, D., Folch, A., Hankin, R. K. S., Caliro, S., Avino, R., and Cardellini, C.: A shallow-layer
460 model for heavy gas dispersion from natural sources: Application and hazard assessment at Caldara di Manziana, Italy, *Geochemistry, Geophysics, Geosystems*, 9, n/a-n/a, <https://doi.org/10.1029/2007GC001762>, 2008.
- Costa, A., Macedonio, G., and Chiodini, G.: Numerical model of gas dispersion emitted from volcanic sources, *Annals of Geophysics*, 48, <https://doi.org/10.4401/ag-3236>, 2009.
- Costa, A., Folch, A., and Macedonio, G.: Density-driven transport in the umbrella region of volcanic clouds: Implications for
465 tephra dispersion models, *Geophys Res Lett*, 40, 4823–4827, <https://doi.org/10.1002/grl.50942>, 2013.
- Dioguardi, F., Massaro, S., Chiodini, G., Costa, A., Folch, A., Macedonio, G., Sandri, L., Selva, J., and Tamburello, G.: VIGIL: A Python tool for automatized probabilistic Volcanic Gas dISpersion modeLling, *Annals of Geophysics*, 65, DM107, <https://doi.org/10.4401/ag-8796>, 2022.
- Douglas, S. G., Kessler, R. C., and Carr, E. L.: User’s guide for the Urban Airshed Model. Volume 3. User’s manual for the
470 Diagnostic Wind Model, San Rafael, CA, 1990.
- Folch, A., Costa, A., and Hankin, R. K. S.: TWODEE-2: A shallow layer model for dense gas dispersion on complex topography, *Comput Geosci*, 35, 667–674, <https://doi.org/10.1016/j.cageo.2007.12.017>, 2009.
- Folch, A., Barcons, J., Kozono, T., and Costa, A.: High-resolution modelling of atmospheric dispersion of dense gas using TWODEE-2.1: application to the 1986 Lake Nyos limnic eruption, *Natural Hazards and Earth System Sciences*, 17, 861–879,
475 <https://doi.org/10.5194/nhess-17-861-2017>, 2017.
- Frezzotti, M. L., Peccerillo, A., and Panza, G.: Carbonate metasomatism and CO₂ lithosphere–asthenosphere degassing beneath the Western Mediterranean: An integrated model arising from petrological and geophysical data, *Chem Geol*, 262, 108–120, <https://doi.org/10.1016/j.chemgeo.2009.02.015>, 2009.
- Gambino, N.: La Mefite nella Valle d’Ansanto di Vincenzo Maria Santoli: rilettura dopo duecento anni: 1783-1983,
480 Tipografica Grafica Amodeo, Avellino, Italy, 424 pp., 1991.
- Granieri, D., Costa, A., Macedonio, G., Bisson, M., and Chiodini, G.: Carbon dioxide in the urban area of Naples: Contribution and effects of the volcanic source, *Journal of Volcanology and Geothermal Research*, 260, 52–61, <https://doi.org/10.1016/j.jvolgeores.2013.05.003>, 2013.
- Hankin, R. K. S. and Britter, R. E.: TWODEE: the Health and Safety Laboratory’s shallow layer model for heavy gas dispersion
485 Part 3: Experimental validation (Thorney Island), *J Hazard Mater*, 66, 239–261, [https://doi.org/10.1016/S0304-3894\(98\)00270-2](https://doi.org/10.1016/S0304-3894(98)00270-2), 1999.
- Hersbach, H., Bell, B., Berrisford, P., Biavati, G., Horányi, A., Muñoz Sabater, J., Nicolas, J., Peubey, C., Radu, R., Rozum, I., Schepers, D., Simmons, A., Soci, C., Dee, D., and Thépaut, J.-N.: ERA5 hourly data on pressure levels from 1940 to present. Copernicus Climate Change Service (C3S) Climate Data Store (CDS). (Accessed on 28-JUL-2023), 2018a.



- 490 Hersbach, H., Bell, B., Berrisford, P., Biavati, G., Horányi, A., Muñoz Sabater, J., Nicolas, J., Peubey, C., Radu, R., Rozum, I., Schepers, D., Simmons, A., Soci, C., Dee, D., and Thépaut, J.-N.: ERA5 hourly data on single levels from 1940 to present. Copernicus Climate Change Service (C3S) Climate Data Store (CDS). (Accessed on 28-JUL-2023), <https://doi.org/https://doi.org/10.24381/cds.adbb2d47>, 2018b.
- Italiano, F., Martelli, M., Martinelli, G., and Nuccio, P. M.: Geochemical evidence of melt intrusions along lithospheric faults
495 of the Southern Apennines, Italy: Geodynamic and seismogenic implications, *J Geophys Res Solid Earth*, 105, 13569–13578, <https://doi.org/10.1029/2000JB900047>, 2000.
- Di Luccio, F., Palano, M., Chiodini, G., Cucci, L., Piromallo, C., Sparacino, F., Ventura, G., Improta, L., Cardellini, C., Persaud, P., Pizzino, L., Calderoni, G., Castellano, C., Cianchini, G., Cianetti, S., Cinti, D., Cusano, P., De Gori, P., De Santis, A., Del Gaudio, P., Diaferia, G., Esposito, A., Galluzzo, D., Galvani, A., Gasparini, A., Gaudiosi, G., Gervasi, A., Giunchi,
500 C., La Rocca, M., Milano, G., Morabito, S., Nardone, L., Orlando, M., Petrosino, S., Piccinini, D., Pietrantonio, G., Piscini, A., Roselli, P., Sabbagh, D., Sciarra, A., Scognamiglio, L., Sepe, V., Tertulliani, A., Tondi, R., Valoroso, L., Voltattorni, N., and Zuccarello, L.: Geodynamics, geophysical and geochemical observations, and the role of CO₂ degassing in the Apennines, *Earth Sci Rev*, 234, 104236, <https://doi.org/10.1016/j.earscirev.2022.104236>, 2022.
- Magill, C. and Blong, R.: Volcanic risk ranking for Auckland, New Zealand. I: Methodology and hazard investigation, *Bull
505 Volcanol*, 67, 331–339, <https://doi.org/10.1007/s00445-004-0374-6>, 2005.
- Martí, J., Aspinall, W. P., Sobradelo, R., Felpeto, A., Geyer, A., Ortiz, R., Baxter, P., Cole, P., Pacheco, J., Blanco, M. J., and Lopez, C.: A long-term volcanic hazard event tree for Teide-Pico Viejo stratovolcanoes (Tenerife, Canary Islands), *Journal of Volcanology and Geothermal Research*, 178, 543–552, <https://doi.org/10.1016/j.jvolgeores.2008.09.023>, 2008.
- Marzocchi, W., Sandri, L., and Selva, J.: BET_VH: a probabilistic tool for long-term volcanic hazard assessment, *Bull
510 Volcanol*, 72, 705–716, <https://doi.org/10.1007/s00445-010-0357-8>, 2010.
- Massaro, S., Dioguardi, F., Sandri, L., Tamburello, G., Selva, J., Moune, S., Jessop, D. E., Moretti, R., Komorowski, J.-C., and Costa, A.: Testing gas dispersion modelling: A case study at La Soufrière volcano (Guadeloupe, Lesser Antilles), *Journal of Volcanology and Geothermal Research*, 417, 107312, <https://doi.org/10.1016/j.jvolgeores.2021.107312>, 2021.
- Mead, S., Procter, J., Bebbington, M., and Rodriguez-Gomez, C.: Probabilistic Volcanic Hazard Assessment for National Park
515 Infrastructure Proximal to Taranaki Volcano (New Zealand), *Front Earth Sci (Lausanne)*, 10, <https://doi.org/10.3389/feart.2022.832531>, 2022.
- Mostardini, F. and Merlini, S.: Appennino centro-meridionale. Sezioni geologiche e proposta di modello strutturale, *Memorie della Società Geologica Italiana*, 35, 177–202, 1986.
- NCEP (National Centers for Environmental Prediction): National Centers for Environmental Prediction: The Global Forecast
520 System (GFS)-Global Spectral Model (GSM).
- Neri, A., Aspinall, W. P., Cioni, R., Bertagnini, A., Baxter, P. J., Zuccaro, G., Andronico, D., Barsotti, S., Cole, P. D., Esposti Ongaro, T., Hincks, T. K., Macedonio, G., Papale, P., Rosi, M., Santacroce, R., and Woo, G.: Developing an Event Tree for



- probabilistic hazard and risk assessment at Vesuvius, *Journal of Volcanology and Geothermal Research*, 178, 397–415, <https://doi.org/10.1016/j.jvolgeores.2008.05.014>, 2008.
- 525 <https://www.osha.gov/hydrogen-sulfide/>: <https://www.osha.gov/hydrogen-sulfide/>, last access: 25 November 2023.
- Olafsdottir, S. and Gardarsson, S. M.: Impacts of meteorological factors on hydrogen sulfide concentration downwind of geothermal power plants, *Atmos Environ*, 77, 185–192, <https://doi.org/10.1016/j.atmosenv.2013.04.077>, 2013.
- Sandri, L., Thouret, J.-C., Constantinescu, R., Biass, S., and Tonini, R.: Long-term multi-hazard assessment for El Misti volcano (Peru), *Bull Volcanol*, 76, 771, <https://doi.org/10.1007/s00445-013-0771-9>, 2014.
- 530 Selva, J., Costa, A., Marzocchi, W., and Sandri, L.: BET_VH: exploring the influence of natural uncertainties on long-term hazard from tephra fallout at Campi Flegrei (Italy), *Bull Volcanol*, 72, 717–733, <https://doi.org/10.1007/s00445-010-0358-7>, 2010.
- Selva, J., Costa, A., De Natale, G., Di Vito, M. A., Isaia, R., and Macedonio, G.: Sensitivity test and ensemble hazard assessment for tephra fallout at Campi Flegrei, Italy, *Journal of Volcanology and Geothermal Research*, 351, 1–28, <https://doi.org/10.1016/j.jvolgeores.2017.11.024>, 2018.
- 535 Settimo, G., Bertinato, L., Martuzzi, M., Inglessis, M., Paolo" D'ancona, F. ", and Soggiu, M. E.: NOTA TECNICA AD INTERIM Monitoraggio della CO₂ per prevenzione e gestione negli ambienti indoor in relazione alla trasmissione dell'infezione da virus SARS-CoV-2, 2022.
- <https://www.cdc.gov/niosh/idlh/default.html>: <https://www.cdc.gov/niosh/idlh/default.html>, last access: 25 November 2023.
- 540 <https://www.cdc.gov/niosh/npg/npgd0337.html>: <https://www.cdc.gov/niosh/npg/npgd0337.html>, last access: 25 November 2023.
- Tierz, P., Sandri, L., Costa, A., Sulpizio, R., Zaccarelli, L., Di Vito, M. A., and Marzocchi, W.: Uncertainty Assessment of Pyroclastic Density Currents at Mount Vesuvius (Italy) Simulated Through the Energy Cone Model, in: *Natural Hazard Uncertainty Assessment: Modeling and Decision Support*, edited by: Riley, K., Webley, P., and Thompson, M., American
- 545 Geophysical Union, 125–145, <https://doi.org/10.1002/9781119028116.ch9>, 2016.